
SpikeCP: Delay-Adaptive Reliable Spiking Neural Networks via Conformal Prediction

Jiechen Chen, Sangwoo Park, Osvaldo Simeone

King’s Communications, Learning and Information Processing (KCLIP) Lab
 Department of Engineering, King’s College London
 London, WC2R 2LS, United Kingdom
 {jiechen.chen, sangwoo.park, osvaldo.simeone}@kcl.ac.uk

Abstract

Spiking neural networks (SNNs) process time-series data via internal event-driven neural dynamics whose energy consumption depends on the number of spikes exchanged between neurons over the course of the input presentation. In typical implementations of an SNN classifier, decisions are produced after the entire input sequence has been processed, resulting in latency and energy consumption levels that are fairly uniform across inputs. Recently introduced delay-adaptive SNNs tailor the inference latency – and, with it, the energy consumption – to the difficulty of each example, by producing an early decision when the SNN model is sufficiently “confident”. In this paper, we start by observing that, as an SNN processes input samples, its classification decisions tend to be first under-confident and then over-confident with respect to the decision’s ground-truth, unknown, test accuracy. This makes it difficult to determine a stopping time that ensures a desired level of accuracy. To address this problem, we introduce a novel delay-adaptive SNN-based inference methodology that, wrapping around any pre-trained SNN classifier, provides guaranteed reliability for the decisions produced at input-dependent stopping times. The approach entails minimal added complexity as compared to the underlying SNN, requiring only thresholding and counting operations at run time, and it leverages tools from conformal prediction (CP).

1 Introduction

Spiking neural networks (SNNs) have emerged as efficient models for the processing of time series data, particularly in settings characterized by sparse inputs (Davies et al., 2018). SNNs implement recurrent, event-driven, neural dynamics whose energy consumption depends on the number of spikes exchanged between neurons over the course of the input presentation. As shown in Fig. 1(a), an SNN-based classifier processes input time series to produce spiking signals – one for each possible class – with the spiking rate of each output signal typically quantifying the confidence the model has in the corresponding labels. Recently introduced *delay-adaptive* SNN classifiers (Li et al., 2023a,b) tailor the inference latency – and, with it, the energy consumption – to the difficulty of each example. This is done by producing an *early decision* when the SNN model is sufficiently “confident”. This paper addresses the observation that, in practice, the confidence levels output by an SNN, even when adjusted with limited calibration data as in (Li et al., 2021), are not well calibrated, yielding test accuracies at the stopping time that do not meet desired target levels.

To illustrate this problem, Fig. 1(b) shows the test accuracy and confidence level (averaged over test inputs) that are produced by a pre-trained SNN for an image classification task (on the MNIST-DVS dataset (Serrano-Gotarredona and Linares-Barranco, 2015)) as a function of time t . It is observed that the SNN’s classification decisions tend to be first *under-confident* and then *over-confident* with respect to the decision’s ground-truth, unknown, test accuracy. Therefore, relying on the SNN confidence level to decide when to make a decision generally causes a *reliability gap* between the true test accuracy and the target accuracy. This problem can be mitigated by relying on *calibration data* to re-calibrate the SNN confidence level, but only if one has enough calibration data (Li et al., 2021) (see Sec. 6 for experimental evidence, e.g., in Fig. 3).

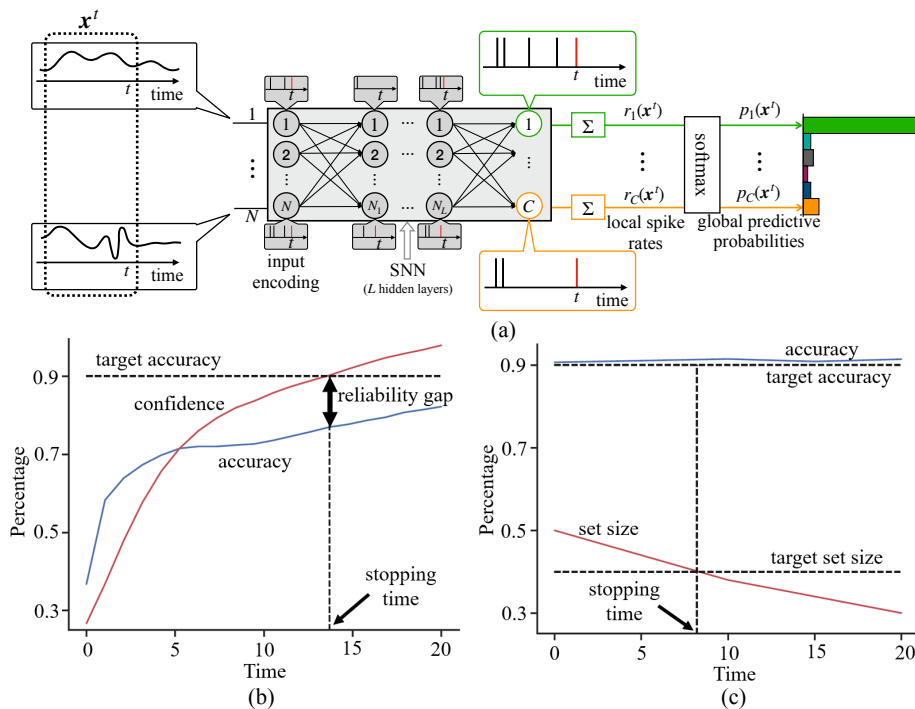


Figure 1: (a) SNN C -class classification model: At time t , real-valued discrete-time time-series data \mathbf{x}^t are fed to the input neurons of an SNN and processed by internal spiking neurons, whose spikes feed C readout neurons. Each output neuron $c \in \{1, \dots, C\}$ evaluates the *local spike count* variable $r_c(\mathbf{x}^t)$ by accumulating the number of spikes it produces. The spike rates may be aggregated across all output neurons to produce the *predictive probability vector* $\{p_c(\mathbf{x}^t)\}_{c=1}^C$. (b) Evolution of confidence and accuracy as a function of time t for a conventional pre-trained SNN. As illustrated, SNN classifiers tend to be first under-confident and then over-confident with respect to the true accuracy, which may cause a positive *reliability gap*, i.e., a shortfall in accuracy, when the confidence level is used as an inference-stopping criterion. (c) Evolution of the (test-averaged) predicted set size (normalized by the number of classes $C = 10$) and of the set accuracy as a function of time t for the same pre-trained SNN when used in conjunction with the proposed SpikeCP method. The set accuracy is the probability that the true label lies inside the predicted set. It is observed that, irrespective of the stopping time, the set accuracy is always guaranteed to exceed the target accuracy level. Therefore, the inference-stopping criterion can be designed to control the trade-off between latency, and hence also energy consumption, and the size of the predicted set.

In this paper, we introduce a novel delay-adaptive SNN solution that (i) provides *guaranteed* reliability – and hence a zero (or non-positive) reliability gap; while (ii) supporting a tunable trade-off between latency and inference energy, on the one hand, and informativeness of the decision, on the other hand. The proposed method, referred to as *SpikeCP*, turns any pre-trained SNN classifier into a *set predictor*, with minimal added complexity, and it leverages tools from *conformal prediction* (CP) (Vovk et al., 2022; Angelopoulos and Bates, 2021).

SpikeCP uses local or global information produced by the output layer of SNN model (see Fig. 1(a)), along with *calibration data*, to produce at each time t a *subset of labels* as its decision. By the properties of CP, the predictive set produced by SpikeCP is shown in this paper to include ground-truth label with any target accuracy level at any stopping time. As illustrated in

Fig. 1(c), this implies that the reliability gap is zero (or negative) for any stopping time. A stopping decision is then made by SpikeCP not based on a reliability requirement – which is always satisfied – but rather based on the desired size of the predicted set. The desired set size provides a novel degree of freedom that can be used to control the trade-off between latency, or energy consumption, and *informativeness* of the decision, as measured by the set size.

2 Problem Definition

In this paper, we consider the problem of efficiently and reliably classifying time series via SNNs by integrating adaptive-latency decision rules (Li et al., 2023a,b) with CP (Vovk et al., 2022; Angelopoulos and Bates, 2021). The proposed scheme, SpikeCP, produces *adaptive SNN-based set classifiers* with *formal reliability*

guarantees. In this section, we start by defining the problem under study, along with the main performance metrics of interest, namely reliability, latency, and inference energy.

2.1 Multi-Class Time Series Classification

We focus on the problem of classifying real-valued vector time series $\mathbf{x} = (\mathbf{x}_1, \dots, \mathbf{x}_T)$, with $N \times 1$ vector samples \mathbf{x}_t over time index $t = 1, \dots, T$, into C classes, using *dynamic* classifiers implemented via SNNs. As illustrated in Fig. 1(a), the SNN model has N input neurons, an arbitrary number of internal spiking neurons; and C output neurons in the readout layer. Each output neuron is associated with one of the C class labels in set $\mathcal{C} = \{1, \dots, C\}$. As detailed in the Supplementary Material, we adopt a standard model based on leaky-integrate-and-fire (LIF) neurons (see, e.g., (Chen et al., 2023b,a,c)).

At each time t , the SNN takes as input the real-valued vector \mathbf{x}_t , and produces sequentially the binary, “spiking”, output vector $\mathbf{y}_t = [y_{t,1}, \dots, y_{t,C}]$ of size C , with $y_{t,c} \in \{0, 1\}$, as a function of the samples

$$\mathbf{x}^t = (\mathbf{x}_1, \dots, \mathbf{x}_t), \quad (1)$$

observed so far. Accordingly, if $y_{t,c} = 1$, output neuron $c \in \mathcal{C}$ emits a spike, while, if $y_{t,c} = 0$, output neuron c is silent. Using conventional *rate decoding*, each output neuron $c \in \mathcal{C}$ maintains the sum of spikes evaluated so far, i.e.,

$$r_c(\mathbf{x}^t) = \sum_{t'=1}^t y_{t',c}, \quad (2)$$

along the time axis $t = 1, \dots, T$.

Each *spike count* variable $r_c(\mathbf{x}^t)$ may be used as an estimate of the degree of confidence of the SNN in class c being the correct one. In order to obtain predictive probabilities, the spike count vector $\mathbf{r}(\mathbf{x}^t) = [r_1(\mathbf{x}^t), \dots, r_C(\mathbf{x}^t)]$ can be passed through a softmax function to yield a probability for class c as $p_c(\mathbf{x}^t) = e^{r_c(\mathbf{x}^t)} / \sum_{c'=1}^C e^{r_{c'}(\mathbf{x}^t)}$ (see Fig. 1(a)). The resulting *predictive probability vector*

$$\mathbf{p}(\mathbf{x}^t) = [p_1(\mathbf{x}^t), \dots, p_C(\mathbf{x}^t)], \quad (3)$$

quantifies the *normalized* confidence levels of the classifier in each class c given the observations up to time t . We emphasize that evaluating the vector (3) requires coordination among all output neurons, since each probability value $p_c(\mathbf{x}^t)$ depends on the spike counts of all output spiking neurons.

A classifier is said to be *well calibrated* if the confidence vector $\mathbf{p}(\mathbf{x}^t)$ provides a close approximation of the true, test, accuracy of each decision $c \in \mathcal{C}$. Machine

Table 1: Taxonomy of SNN classifiers

adaptivity		
decision type	non-adaptive	adaptive
point	conventional (e.g., (Jang et al., 2019))	DC-SNN (Li et al., 2023a), SEENN (Li et al., 2023b)
set	SpikeCP (this work)	SpikeCP (this work)

learning models based on deep learning are well known to be typically *over-confident*, resulting in confidence vectors $\mathbf{p}(\mathbf{x}^t)$ that are excessively skewed towards a single class c , dependent on the input \mathbf{x}^t (Guo et al., 2017; Sun et al., 2023). As discussed in Sec. 1, SNN models also tend to provide over-confident decisions as time t increases.

Following the conventional supervised learning formulation of the problem, multi-class time series classification data consist of pairs (\mathbf{x}, c) of input sequence \mathbf{x} and true class index $c \in \mathcal{C}$. All data points are generated from a *ground-truth distribution* $p(\mathbf{x}, c)$ in an independent and identically distributed (i.i.d.) manner. We focus on *pre-trained* SNN classification models, on which we make no assumptions in terms of accuracy or calibration. Furthermore, we assume the availability of a, typically small, *calibration data set*

$$\mathcal{D}^{\text{cal}} = \{\mathbf{z}[i] = (\mathbf{x}[i], c[i])\}_{i=1}^{|\mathcal{D}^{\text{cal}}|}. \quad (4)$$

In practice, a new calibration data set may be produced periodically at test time to be reused across multiple test points (\mathbf{x}, c) (Li et al., 2023a; Vovk et al., 2022; Angelopoulos and Bates, 2021).

2.2 Taxonomy of SNN Classifiers

As detailed in Table 1 and Fig. 2, we distinguish SNN classifiers along two axes, namely adaptivity and decision type.

Adaptivity: As shown in Fig. 2(a) and Fig. 2(c), a *non-adaptive* classifier, having observed all the T samples of the input sequence \mathbf{x} , makes a decision on the basis of the spike count vector $\mathbf{r}(\mathbf{x}^T) = \mathbf{r}(\mathbf{x})$ or of the predictive probability vector $\mathbf{p}(\mathbf{x}^T) = \mathbf{p}(\mathbf{x})$. In contrast, as seen Fig. 2(b) and Fig. 2(d), an *adaptive* classifier allows for the time $T_s(\mathbf{x})$ at which a classification decision is produced, to be adapted to the difficulty of the input \mathbf{x} . For any given input \mathbf{x} , the *stopping time* $T_s(\mathbf{x})$ and the final decision produced at time $T_s(\mathbf{x})$ depend on either the spike count vector $\mathbf{r}(\mathbf{x}^t)$ or on the predictive distribution vector $\mathbf{p}(\mathbf{x}^t)$ produced by the

SNN classifier after having observed the first $t = T_s(\mathbf{x})$ input samples \mathbf{x}^t in (1).

Decision type: As illustrated in Fig. 2(a) and Fig. 2(b), for any given input \mathbf{x} , a conventional *point classifier* produces as output a single estimate $\hat{c}(\mathbf{x})$ of the label c in a non-adaptive (Fig. 2(a)) or adaptive (Fig. 2(b)) way. In contrast, as seen in Fig. 2(c) and Fig. 2(d), a *set classifier* outputs a decision in the form of a *subset* $\Gamma(\mathbf{x}) \subseteq \mathcal{C}$ of the C classes (Vovk et al., 2022; Angelopoulos and Bates, 2021), with the decision being non-adaptive (Fig. 2(c)) or adaptive (Fig. 2(d)). The *predicted set* $\Gamma(\mathbf{x})$ describes the classifier’s estimate of the most likely candidate labels for input \mathbf{x} . Accordingly, a predicted set $\Gamma(\mathbf{x})$ with a larger cardinality $|\Gamma(\mathbf{x})|$ is less *informative* than one with a smaller (but non-zero) cardinality.

2.3 Reliability, Latency, and Inference Energy

In this work, we study the performance of adaptive classifiers on the basis of the following metrics.

Reliability: Given a *target accuracy level* $p_{\text{targ}} \in (0, 1)$, an adaptive *point classifier* is said to be *reliable* if the accuracy of its decision is no smaller than the target level p_{targ} . This condition is stated as

$$\begin{aligned} \Pr(c = \hat{c}(\mathbf{x})) &\geq p_{\text{targ}}, \\ \text{i.e., } \Delta R = p_{\text{targ}} - \Pr(c = \hat{c}(\mathbf{x})) &\leq 0, \end{aligned} \quad (5)$$

where $\hat{c}(\mathbf{x})$ is the decision made by the adaptive point classifier at time $T_s(\mathbf{x})$ (see Fig. 2(b)). In (5), we have defined the *reliability gap* ΔR , which is positive for *unreliable* classifiers and non-positive for *reliable* ones (see Fig. 1(b)). In a similar manner, an adaptive *set predictor* $\Gamma(\mathbf{x})$ is reliable at the target accuracy level p_{targ} if the true class c is included in the predicted set $\Gamma(\mathbf{x})$, produced at the stopping time $T_s(\mathbf{x})$, with probability no smaller than the desired accuracy level p_{targ} . This is written as

$$\begin{aligned} \Pr(c \in \Gamma(\mathbf{x})) &\geq p_{\text{targ}}, \\ \text{i.e. } \Delta R = p_{\text{targ}} - \Pr(c \in \Gamma(\mathbf{x})) &\leq 0, \end{aligned} \quad (6)$$

where $\Gamma(\mathbf{x})$ is the decision made by the adaptive set classifier at time $T_s(\mathbf{x})$ (see Fig. 2(d)). The probabilities in (5) and (6) are taken over the distribution of the test data point (\mathbf{x}, c) and of the calibration data (4).

Latency: Latency is defined as the average stopping time $\mathbb{E}[T_s(\mathbf{x})]$, where the expectation is taken over the same distribution as for (5) and (6).

Inference energy: As a proxy for the energy consumption of the SNN classifier at inference time, we follow the standard approach also adopted in, e.g., (Chen

et al., 2023b,a; Davies, 2018), of counting the average number of spikes, denoted as $\mathbb{E}[S(\mathbf{x})]$, that are produced internally by the SNN classifier prior to producing a decision.

3 Adaptive Point Classification

In this section, we review, for reference, the adaptive point classifier introduced in (Li et al., 2023a), which is referred to as *dynamic-confidence SNN* (DC-SNN). We note that another adaptive point classifier was introduced in (Li et al., 2023b), which requires the implementation of a separate artificial neural network (ANN) to find the stopping time $T_s(\mathbf{x})$ as a function of the entire input sequence \mathbf{x} . Due to its different requirements in terms of models and input presentation, we leave a comparison with this scheme, referred to as here *stopping policy-SNN* (SP-SNN), to the Supplementary Material.

As illustrated in Fig. 2(b), DC-SNN produces a decision at the first time t for which the maximum confidence level across all possible classes is larger than a fixed *target confidence level* $p_{\text{th}} \in (0, 1)$. Accordingly, the stopping time is given by

$$T_s(\mathbf{x}) = \min_{t \in \{1, \dots, T\}} t \text{ s.t. } \max_{c \in \mathcal{C}} p_c(\mathbf{x}^t) \geq p_{\text{th}}, \quad (7)$$

if there is a time $t < T$ that satisfies the constraint; and $T_s(\mathbf{x}) = T$ otherwise. The rationale for this approach is that, by (7), if $T_s(\mathbf{x}) < T$, the classifier has a confidence level no smaller than p_{th} on the decision

$$\hat{c}(\mathbf{x}) = \arg \max_{c \in \mathcal{C}} p_c(\mathbf{x}^{T_s(\mathbf{x})}). \quad (8)$$

If the SNN classifier is *well calibrated*, the confidence level coincides with the true accuracy of the decision given by the class $\arg \max_{c \in \mathcal{C}} p_c(\mathbf{x}^t)$ at all times t . Therefore, setting the target confidence level p_{th} to be equal to the target accuracy p_{targ} , i.e., $p_{\text{th}} = p_{\text{targ}}$, guarantees a zero, or negative, reliability gap for the adaptive decision (8) when $T_s(\mathbf{x}) < T$. However, as discussed in Sec. 1, the assumption of calibration is typically not valid (see Fig. 1(b)). To address this problem, (Li et al., 2023a) introduced a solution based on the use of a calibration data set.

Specifically, DC-SNN evaluates the empirical accuracy of the decision (8), i.e., $\hat{\mathcal{A}}^{\text{cal}}(p_{\text{th}}) = |\mathcal{D}^{\text{cal}}|^{-1} \sum_{i=1}^{|\mathcal{D}^{\text{cal}}|} \mathbb{1}(\hat{c}(\mathbf{x}[i]) = c[i])$, where $\mathbb{1}(\cdot)$ is the indicator function, for a grid of possible values of the target confidence level p_{th} . Then, it chooses the minimum value p_{th} that ensures the inequality $\hat{\mathcal{A}}^{\text{cal}}(p_{\text{th}}) \geq p_{\text{targ}}$, so that the calibration accuracy exceeds the target accuracy level p_{targ} ; or the smallest value p_{th} that maximizes $\hat{\mathcal{A}}^{\text{cal}}(p_{\text{th}})$ if the constant $\hat{\mathcal{A}}^{\text{cal}}(p_{\text{th}}) \geq p_{\text{targ}}$ cannot be met.

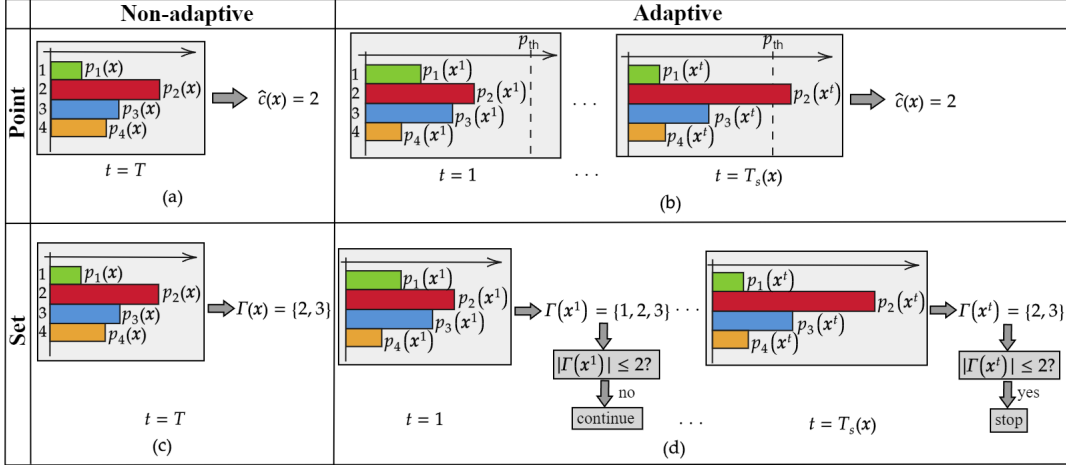


Figure 2: (a) A *non-adaptive point* classifier outputs a point decision $\hat{c}(\mathbf{x})$ after having observed the entire time series \mathbf{x} . (b) An *adaptive point* classifier stops when the confidence level of the classifier passes a given threshold p_{th} , producing a classification decision at an input-dependent time $T_s(\mathbf{x})$. (c) A *non-adaptive set* classifier produces a predicted set $\Gamma(\mathbf{x})$ consisting of a subset of the class labels after having observed the entire time series \mathbf{x} . (d) The *adaptive set* classifiers presented in this work stop at the earliest time $T_s(\mathbf{x})$ when the predicted set $\Gamma(\mathbf{x}^{T_s(\mathbf{x})})$ is sufficiently informative, in the sense that its cardinality is below a given threshold I_{th} (in the figure we set $I_{\text{th}} = 2$). The proposed SpikeCP method can guarantee that the predicted set $\Gamma(\mathbf{x}) = \Gamma(\mathbf{x}^{T_s(\mathbf{x})})$ at the stopping time $T_s(\mathbf{x})$ includes the true label with probability no smaller than the target probability p_{target} .

4 SpikeCP: Reliable Adaptive Set Classification

The adaptive point classifiers reviewed in the previous section are generally characterized by a positive reliability gap (see Fig. 1(a)), unless the underlying SNN classifier is well calibrated or unless the calibration data set is large enough to ensure a reliable estimate of the true accuracy. In this section, we introduce *SpikeCP*, a novel inference methodology for adaptive classification that wraps around any pre-trained SNN model, guaranteeing the reliability requirement (6) – and hence a zero, or negative, reliability gap – irrespective of the quality of the SNN classifier and of the amount of calibration data.

4.1 Stopping Time

SpikeCP pre-determines a subset of possible stopping times, referred to as *checkpoints*, in set $\mathcal{T}_s \subseteq \{1, \dots, T\}$. Set $\mathcal{T}_s \subseteq \{1, \dots, T\}$ always includes the last time T , and adaptivity is only possible if the cardinality of set \mathcal{T}_s is strictly larger than one. At each time $t \in \mathcal{T}_s$, using the local spike count variables $\mathbf{r}(\mathbf{x}^t)$ or the global predictive probabilities $\mathbf{p}(\mathbf{x}^t)$, SpikeCP produces a candidate predicted set $\Gamma(\mathbf{x}^t) \subseteq \mathcal{C}$. Then, as illustrated in Fig. 2(d), the cardinality $|\Gamma(\mathbf{x}^t)|$ of the candidate predicted set $\Gamma(\mathbf{x}^t)$ is compared with a threshold I_{th} . If we have the inequality

$$|\Gamma(\mathbf{x}^t)| \leq I_{\text{th}}, \quad (9)$$

the predicted set is deemed to be sufficiently *informative*, and SpikeCP stops processing the input to produce set $\Gamma(\mathbf{x}^t)$ as the final decision $\Gamma(\mathbf{x})$. As we detail next and as illustrated in Fig. 1(c), the candidate predicted sets $\Gamma(\mathbf{x}^t)$ are constructed in such a way to ensure a non-positive reliability gap simultaneously for *all* checkpoints, and hence also at the stopping time.

To construct the candidate predicted set $\Gamma(\mathbf{x}^t)$ at a checkpoint $t \in \mathcal{T}_s$, SpikeCP follows the *split, or validation-based, CP* procedure proposed in (Vovk et al., 2022) and reviewed in (Angelopoulos and Bates, 2021; Tibshirani, 2023). Accordingly, using the local rate counts $\mathbf{r}(\mathbf{x}^t)$ or the global probabilities $\mathbf{p}(\mathbf{x}^t)$, SpikeCP produces a so-called *non-conformity (NC) score* vector $\mathbf{s}(\mathbf{x}^t) = [s_1(\mathbf{x}^t), \dots, s_C(\mathbf{x}^t)]$. Each entry $s_c(\mathbf{x}^t)$ of this vector is a measure of the *lack of confidence* of the SNN classifier in label c given input \mathbf{x}^t . The candidate predicted set $\Gamma(\mathbf{x}^t)$ is then obtained by including all labels $c \in \mathcal{C}$ whose NC score $s_c(\mathbf{x}^t)$ is no larger than a threshold s_{th}^t , i.e.,

$$\Gamma(\mathbf{x}^t) = \{c \in \mathcal{C} : s_c(\mathbf{x}^t) \leq s_{\text{th}}^t\}. \quad (10)$$

As described in Sec. 4.2, the threshold s_{th}^t is evaluated as a function of the target accuracy level p_{target} , of the calibration set \mathcal{D}^{cal} , and of the number of checkpoints $|\mathcal{T}_s|$.

We consider two NC scores, one locally computable at the output neurons and one requiring coordination among the output neurons. The *local NC score* is

defined as

$$s_c(\mathbf{x}^t) = t - r_c(\mathbf{x}^t). \quad (11)$$

Intuitively, class c is assigned a lower NC score (11) – and hence a higher degree of confidence – if the spike count variable $r_c(\mathbf{x}^t)$ is larger. In contrast, the *global NC score* is given by the standard *log-loss*

$$s_c(\mathbf{x}^t) = -\log p_c(\mathbf{x}^t). \quad (12)$$

4.2 Evaluation of the Threshold

As we detail in this subsection, the threshold s_{th}^t in (10) is evaluated based on the calibration data set \mathcal{D}^{cal} , with the goal of ensuring the reliability condition (6) for a target accuracy level p_{targ} . The general methodology follows CP, with the important caveat that, in order to ensure a non-positive reliability gap simultaneously at all checkpoints, a form of *Bonferroni correction* is applied. Let us define as $1 - \alpha$, with $\alpha \in (0, 1)$, an auxiliary *per-checkpoint accuracy level*. Suppose that we can guarantee the *per-checkpoint reliability condition*

$$\Pr(c \in \Gamma(\mathbf{x}^t)) \geq 1 - \alpha \quad (13)$$

for all checkpoints $t \in \mathcal{T}_s$. Then, by the union bound, we also have the reliability condition

$$\Pr(c \in \Gamma(\mathbf{x}^t) \text{ for all } t \in \mathcal{T}_s) \geq 1 - |\mathcal{T}_s|\alpha, \quad (14)$$

which applies simultaneously across all checkpoints. This inequality implies that we can guarantee the condition (6) by setting $\alpha = (1 - p_{\text{targ}})/|\mathcal{T}_s|$, since the stopping point $T_s(\mathbf{x})$ is in set \mathcal{T}_s by construction.

The remaining open question is how to ensure the per-checkpoint reliability condition (13). To address this goal, we follow the standard CP procedure. Accordingly, during an *offline* phase, for each calibration data point $(\mathbf{x}[i], c[i])$, with $i = 1, \dots, |\mathcal{D}^{\text{cal}}|$, SpikeCP computes the NC score $s^t[i] = s_{c[i]}(\mathbf{x}^t[i])$ at each checkpoint $t \in \mathcal{T}_s$. The calibration NC scores $\{s^t[i]\}_{i=1}^{|\mathcal{D}^{\text{cal}}|}$ are ordered from smallest to largest, with ties broken arbitrarily, separately for each checkpoint t . Finally, the threshold s_{th}^t is selected to be approximately equal to the smallest value that is larger than a fraction $(1 - \alpha)$ of the calibration NC scores (see Fig. 3). More precisely, assuming $\alpha \geq 1/(|\mathcal{D}^{\text{cal}}| + 1)$ we set (Vovk et al., 2022; Angelopoulos and Bates, 2021)

$$s_{\text{th}}^t = \lceil (1 - \alpha)(|\mathcal{D}^{\text{cal}}| + 1) \rceil\text{-th} \\ \text{smallest value in the set } \{s^t[i]\}_{i=1}^{|\mathcal{D}^{\text{cal}}|}, \quad (15)$$

while for $\alpha < 1/(|\mathcal{D}^{\text{cal}}| + 1)$ we set $s_{\text{th}}^t = \infty$.

The fact that choice (15) satisfies the condition (13) follows from the assumption that the data points are

i.i.d. In fact, this assumption implies that the NC scores of calibration data points and of a test data point are also i.i.d. In turn, this ensures that the ranking of the test NC score among the $|\mathcal{D}^{\text{cal}}| + 1$ NC scores is uniformly distributed. Finally, this causes the test NC score to be larger than a fraction $1 - \alpha$ of calibration NC scores with a probability no larger than α . We refer to (Angelopoulos and Bates, 2021) for a detailed proof of condition (13).

4.3 Reliability Guarantees of SpikeCP

In line with the intuitive argument given at the end of the last section, the adaptive set predictor $\Gamma(\mathbf{x})$ produced by SpikeCP is guaranteed to satisfy the reliability condition (6), as formalized next.

Theorem 1 (Reliability of SpikeCP). *The adaptive decision $\Gamma(\mathbf{x}) = \Gamma(\mathbf{x}^{T_s(\mathbf{x})})$ produced by SpikeCP, as described in Sec. 4.1–4.2, has a non-positive reliability gap, i.e., $\Delta R \leq 0$, and hence it satisfies the reliability condition (6).*

Proof. The proof follows directly from the properties of CP (see, e.g., (Tibshirani et al., 2019, Theorem 1) and (Vovk et al., 2022; Kuchibhotla, 2020; Lei et al., 2018)). It is noted that the result holds also under the more general assumption that calibration and test data points are *exchangeable* and not necessarily i.i.d. \square

5 Related Work

Training SNNs. Typical training algorithms for SNNs are based on approximations of backpropagation-through-time that simplify credit assignment and address the non-differentiability of the spiking mechanism (Neftci et al., 2019; Woźniak et al., 2020; Davies et al., 2018). Another approach is to model the spiking mechanism as a stochastic process, which enables the use of likelihood-based methods (Jang et al., 2019), as well as of Bayesian rules (Skatchkovsky et al., 2022). SpikeCP works as a wrapper around any training scheme.

Calibration and delay-adaptivity for SNN. Calibration is an underexplored subject for SNNs. SNN calibration is carried out by leveraging a pre-trained ANN in (Li et al., 2021); while (Skatchkovsky et al., 2022) applies Bayesian learning to reduce the calibration error. As discussed in the previous sections, adaptivity for rate decoding was studied in (Li et al., 2023a,b). Other forms of adaptivity may leverage *temporal decoding*, whereby, for instance, as soon as one output neuron spikes a decision is made (Rosenfeld et al., 2019). Extending SpikeCP to time decoding is an interesting direction for future work.

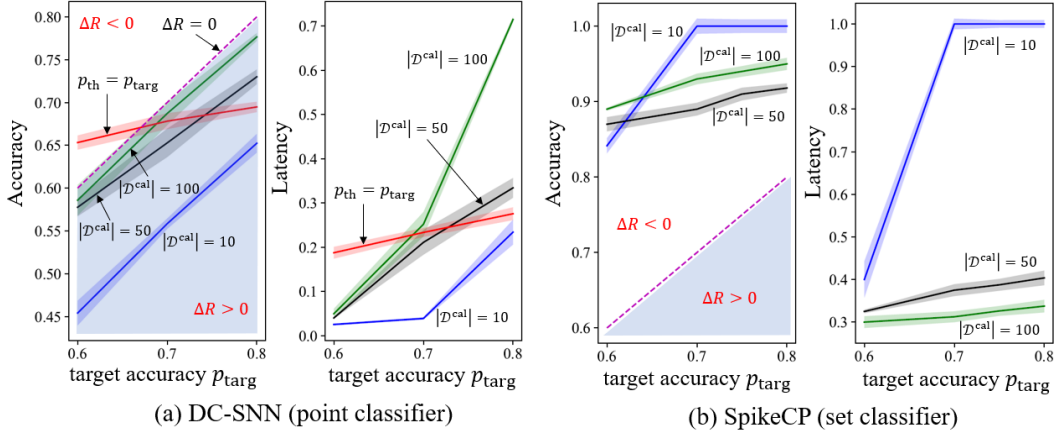


Figure 3: MNIST-DVS experiments: (a) Accuracy $\Pr(c = \hat{c}(\mathbf{x}))$ and normalized latency $\mathbb{E}[T_s(\mathbf{x})]/T$ for the DC-SNN point classifier (Li et al., 2023a); (b) Accuracy $\Pr(c \in \Gamma(\mathbf{x}))$ and normalized latency $\mathbb{E}[T_s(\mathbf{x})]/T$ for the proposed SpikeCP set predictor given the target set size $I_{\text{th}} = 3$. The shaded error bars correspond to intervals covering 95% of the realized values, obtained from 50 different draws of calibration data.

Early exit in conventional deep learning. The idea of delay-adaptivity in SNNs is related to that of *early-exit* decisions in feedforward neural networks. In neural networks with an early exit option, confidence levels are evaluated at intermediate layers, and a decision is made when the confidence level passes a threshold (Panda et al., 2016; Teerapittayanon et al., 2016; Laskaridis et al., 2020). The role of calibration for early-exit neural networks was studied in (Pacheco et al., 2021).

Prediction cascades. Another related concept is that of prediction cascades, which apply a sequence of classifiers, ranging from light-weight to computationally expensive (Weiss and Taskar, 2010), to a static input. The goal is to apply the more expensive classifiers only when the difficulty of the input requires it. The application of CP to prediction cascades was investigated in (Fisch et al., 2020).

6 Experiments

In this section, we provide experimental results for MNIST-DVS dataset (Serrano-Gotarredona and Linares-Barranco, 2015) and the DVS128 Gesture dataset (Amir et al., 2017) by focusing on DC-SNN (Li et al., 2023a) and SpikeCP. The first data set represents an image classification task, and the latter a video recognition task, and both tasks are based on data recorded by a neuromorphic (DVS) camera. Comparisons with SP-SNN (Li et al., 2023b) are reported in the Supplementary Material, which includes also additional results on SpikeCP for the CIFAR-10 dataset. All the experiments were run over a GPU server with single NVIDIA A100 card. Training is done via the surrogate gradient method (Neftci et al., 2019). The calibration data set \mathcal{D}^{cal} is obtained by randomly sam-

pling $|\mathcal{D}^{\text{cal}}|$ examples from the test set, with the rest used for testing (see, e.g., (Angelopoulos et al., 2022)). We adopt the global NC score (12) and refer to the Supplementary Material for a comparison with the local NC score (11).

6.1 MNIST-DVS Dataset

The MNIST-DVS dataset contains time series recorded from a DVS camera that is shown moving handwritten digits from “0” to “9” on a screen. The data set contains 8,000 training examples, as well as 2,000 examples used for calibration and testing. For this experiment, we adopt a fully connected SNN with one hidden layer having 1,000 neurons. The length of the time series is $T = 80$ samples, and we fix the set of possible checkpoints as $\mathcal{T}_s = \{20, 40, 60, 80\}$, and the target set size to $I_{\text{th}} = 3$.

Fig. 3 reports accuracy – $\Pr(c = \hat{c}(\mathbf{x}))$ for DC-SNN and $\Pr(c \in \Gamma(\mathbf{x}))$ for SpikeCP – and normalized latency $\mathbb{E}[T_s(\mathbf{x})]/T$ as a

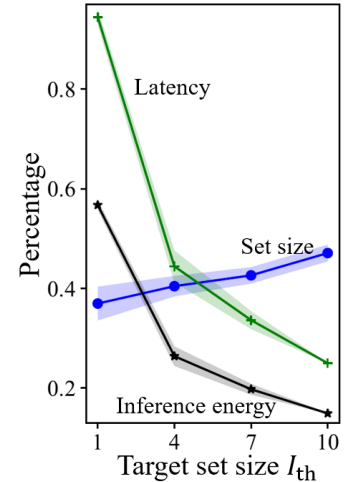


Figure 4: MNIST-DVS experiments: Normalized latency, inference energy, and set size (informativeness) as a function of target set size I_{th} for SpikeCP, assuming $p_{\text{targ}} = 0.9$ and $|\mathcal{D}^{\text{cal}}| = 200$ under the same conditions as Fig. 4.

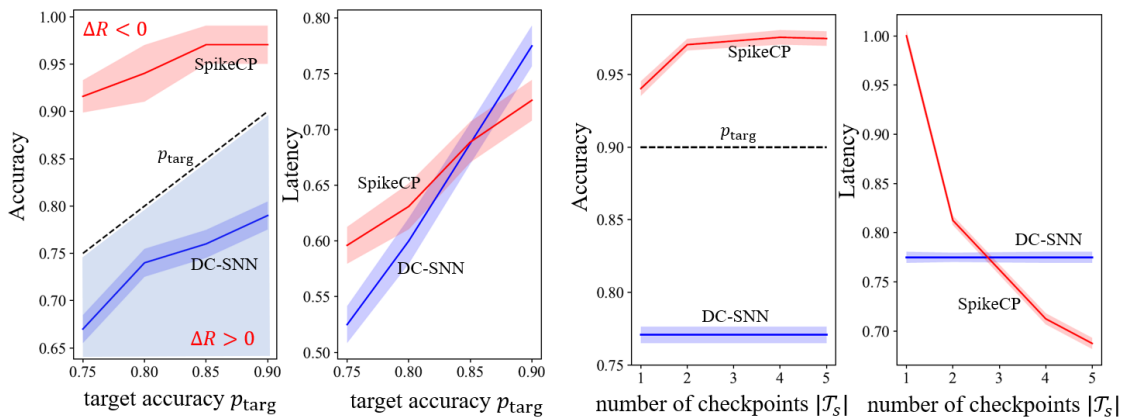


Figure 5: DVS128 Gesture experiments: Accuracy ($\Pr(c = \hat{c}(\mathbf{x}))$) for DC-SNN and $\Pr(c \in \Gamma(\mathbf{x}))$ for SpikeCP), and normalized latency $\mathbb{E}[T_s(\mathbf{x})]/T$ for the proposed SpikeCP set predictor and DC-SNN as a function of target accuracy p_{targ} and the number of checkpoints $|\mathcal{T}_s|$ with $|\mathcal{D}^{\text{cal}}| = 50$, $p_{\text{targ}} = 0.9$, $|\mathcal{T}_s| = 4$ and $I_{\text{th}} = 3$.

function of the target accuracy p_{targ} for different sizes $|\mathcal{D}^{\text{cal}}|$ of the calibration data set. The accuracy plots highlight the regime in which we have a positive reliability gap ΔR in (5) and (6), which corresponds to *unreliable* decisions.

By leveraging calibration data, DC-SNN suitably increases the decision latency as the target probability p_{targ} increases. However, a non-positive reliability gap is only attained by DC-SNN when the number of calibration data points is sufficiently large, here $|\mathcal{D}^{\text{cal}}| = 100$. In contrast, as shown in Fig. 3(b) and proved in Theorem 1, SpikeCP is always reliable, achieving a non-positive reliability gap irrespective of the number of calibration data points. Furthermore, with a fixed threshold I_{th} as in this example, increasing the size $|\mathcal{D}^{\text{cal}}|$ of the calibration data set has the effect of significantly reducing the average latency of DC-SNN.

The trade-off supported by SpikeCP between latency and energy, on the one hand, and informativeness, i.e., set size, on the other hand, is investigated in Fig. 4 by varying the target set size I_{th} , with target accuracy level $p_{\text{targ}} = 0.9$ and $|\mathcal{D}^{\text{cal}}| = 200$ calibration examples. Note that the reliability gap is always negative as in Fig. 3(b), and is hence omitted in the figure to avoid clutter. Increasing the target set size, I_{th} , causes the final predicted set size, shown in the figure normalized by the number of classes $C = 10$, to increase, yielding less informative decisions. On the flip side, sacrificing informativeness entails a lower (normalized) latency, as well as, correspondingly, a lower inference energy, with the latter shown in the figure as the average number of spikes per sample and per hidden neuron, $\mathbb{E}[S(\mathbf{x})]/(1000T)$.

6.2 DVS128 Gesture Dataset

The DVS128 Gesture data set collects videos from a DVS camera that is shown an actor performing one of 11 different gestures under three different illumination conditions. We divide each time series into $T = 80$ time intervals, integrating the discrete samples within each interval to obtain a (continuous-valued) time sample (Fang et al., 2021). The dataset contains 1176 training data and 288 test data, from which 50 examples are chosen to serve as calibration data. The SNN architecture is constructed using a convolutional layer, encompassing batch normalization and max-pooling layer, as well as a fully-connected layer as described in (Fang et al., 2021). We set the set size threshold to $I_{\text{th}} = 3$.

Fig. 5 reports the accuracy and latency for DC-SNN and SpikeCP with different target accuracy p_{targ} and number of checkpoints $|\mathcal{T}_s|$. In a manner consistent with the MNIST-DVS results, DC-SNN fails to meet the target accuracy, despite increasing the latency as p_{targ} increases. In contrast, SpikeCP is reliable, providing a negative reliability gap for all values p_{targ} . Furthermore, increasing the number of checkpoints, $|\mathcal{T}_s|$, the latency of SpikeCP decreases, since the SNN has more, earlier, choices of times at which to stop inference.

7 Conclusions

In this work, we have introduced SpikeCP, a delay-adaptive SNN set predictor with provable reliability guarantees. SpikeCP wraps around any pre-trained SNN classifier, producing a set classifier with a tunable trade-off between informativeness of the decision – i.e., size of the predicted set – and latency, or inference energy as measured by the number of spikes. Unlike prior art, the reliability guarantees of SpikeCP hold irrespective of the quality of the pre-trained SNN and of

the number of calibration points, with minimal added *complexity*. In fact, as summarized in Algorithm 1, at test time, SpikeCP only requires thresholding the rate-decoded outputs of the SNN, and counting the number of classes passing the threshold.

Future work may focus on the derivation of tighter bounds on the simultaneous reliability condition (14) beyond the basic Bonferroni correction applied here. Lastly, extension of SpikeCP to time decoding may further reduce the delay/energy.

References

- Amir, A. et al. (2017). A low power, fully event-based gesture recognition system. In *Proceedings of the IEEE conference on computer vision and pattern recognition*, pages 7243–7252.
- Angelopoulos, A. N. and Bates, S. (2021). A gentle introduction to conformal prediction and distribution-free uncertainty quantification. arXiv 2021. *arXiv preprint arXiv:2107.07511*.
- Angelopoulos, A. N., Bates, S., Fisch, A., Lei, L., and Schuster, T. (2022). Conformal risk control. *arXiv preprint arXiv:2208.02814*.
- Chen, J., Skatchkovsky, N., and Simeone, O. (2023a). Neuromorphic integrated sensing and communications. *IEEE Wireless Communications Letters*, 12(3):476–480.
- Chen, J., Skatchkovsky, N., and Simeone, O. (2023b). Neuromorphic wireless cognition: Event-driven semantic communications for remote inference. *IEEE Transactions on Cognitive Communications and Networking*, 9(2):252–265.
- Chen, L., Jose, S. T., Nikoloska, I., Park, S., Chen, T., Simeone, O., et al. (2023c). Learning with limited samples: Meta-learning and applications to communication systems. *Foundations and Trends® in Signal Processing*, 17(2):79–208.
- Davies, M. (2018). Loihi: A neuromorphic manycore processor with on-chip learning. *IEEE Micro*, 38(1):82–99.
- Davies, M. et al. (2018). Loihi: A neuromorphic manycore processor with on-chip learning. *Ieee Micro*, 38(1):82–99.
- Fang, W., Yu, Z., Chen, Y., Masquelier, T., Huang, T., and Tian, Y. (2021). Incorporating learnable membrane time constant to enhance learning of spiking neural networks. In *Proceedings of the IEEE/CVF international conference on computer vision*, pages 2661–2671.
- Fisch, A., Schuster, T., Jaakkola, T., and Barzilay, R. (2020). Efficient conformal prediction via cascaded inference with expanded admission. *arXiv preprint arXiv:2007.03114*.
- Gerstner, W. and Kistler, W. M. (2002). *Spiking neuron models: Single neurons, populations, plasticity*. Cambridge University Press.
- Guo, C., Pleiss, G., Sun, Y., and Weinberger, K. Q. (2017). On calibration of modern neural networks. In *International conference on machine learning*, pages 1321–1330. PMLR.
- Jang, H., Simeone, O., Gardner, B., and Gruning, A. (2019). An introduction to probabilistic spiking neural networks: Probabilistic models, learning rules, and applications. *IEEE Signal Processing Magazine*, 36(6):64–77.
- Kuchibhotla, A. K. (2020). Exchangeability, conformal prediction, and rank tests. *arXiv preprint arXiv:2005.06095*.
- Laskaridis, S., Venieris, S. I., Almeida, M., Leontiadis, I., and Lane, N. D. (2020). Spinn: synergistic progressive inference of neural networks over device and cloud. In *Proceedings of the 26th annual international conference on mobile computing and networking*, pages 1–15.
- Lei, J., G’Sell, M., Rinaldo, A., Tibshirani, R. J., and Wasserman, L. (2018). Distribution-free predictive inference for regression. *Journal of the American Statistical Association*, 113(523):1094–1111.
- Li, C., Jones, E., and Furber, S. (2023a). Unleashing the potential of spiking neural networks by dynamic confidence. *arXiv preprint arXiv:2303.10276*.
- Li, Y., Deng, S., Dong, X., Gong, R., and Gu, S. (2021). A free lunch from ANN: Towards efficient, accurate spiking neural networks calibration. In *International Conference on Machine Learning*, pages 6316–6325. PMLR.
- Li, Y., Geller, T., Kim, Y., and Panda, P. (2023b). SEENN: Towards temporal spiking early-exit neural networks. *arXiv preprint arXiv:2304.01230*.
- Neftci, E. O., Mostafa, H., and Zenke, F. (2019). Surrogate gradient learning in spiking neural networks: Bringing the power of gradient-based optimization to spiking neural networks. *IEEE Signal Processing Magazine*, 36(6):51–63.
- Pacheco, R. G., Couto, R. S., and Simeone, O. (2021). Calibration-aided edge inference offloading via adaptive model partitioning of deep neural networks. In *ICC 2021-IEEE International Conference on Communications*, pages 1–6. IEEE.
- Panda, P., Sengupta, A., and Roy, K. (2016). Conditional deep learning for energy-efficient and enhanced pattern recognition. In *2016 Design, Automation & Test in Europe Conference & Exhibition (DATE)*, pages 475–480. IEEE.
- Rosenfeld, B., Simeone, O., and Rajendran, B. (2019). Learning first-to-spike policies for neuromorphic control using policy gradients. In *2019 IEEE 20th International Workshop on Signal Processing Advances in Wireless Communications (SPAWC)*, pages 1–5. IEEE.
- Serrano-Gotarredona, T. and Linares-Barranco, B. (2015). Poker-DVS and MNIST-DVS. their history, how they were made, and other details. *Frontiers in neuroscience*, 9:481.
- Skatchkovsky, N., Jang, H., and Simeone, O. (2022). Bayesian continual learning via spiking neural networks. *arXiv preprint arXiv:2208.13723*.
- Sun, T., Yin, B., and Bohte, S. (2023). Efficient uncertainty estimation in spiking neural networks via mc-dropout. *arXiv preprint arXiv:2304.10191*.
- Teerapittayanon, S., McDanel, B., and Kung, H.-T. (2016). Branchynet: Fast inference via early exiting from deep neural networks. In *2016 23rd International Conference on Pattern Recognition (ICPR)*, pages 2464–2469. IEEE.
- Tibshirani, R. (2023). *Conformal Prediction: Advanced Topics in Statistical Learning (Lecture note)*.
- Tibshirani, R. J., Foygel Barber, R., Candès, E., and Ramdas, A. (2019). Conformal prediction under covariate

shift. *Advances in neural information processing systems*, 32.

Vovk, V., Gammerman, A., and Shafer, G. (2022). *Algorithmic Learning in a Random World*. Springer Nature.

Weiss, D. and Taskar, B. (2010). Structured prediction cascades. In *Proceedings of the Thirteenth International Conference on Artificial Intelligence and Statistics*, pages 916–923. JMLR Workshop and Conference Proceedings.

Woźniak, S., Pantazi, A., Bohnstingl, T., and Eleftheriou, E. (2020). Deep learning incorporating biologically inspired neural dynamics and in-memory computing. *Nature Machine Intelligence*, 2(6):325–336.

Supplementary A.1 Spiking Neural Network Model

In this work, we adopt the standard leaky-integrate-and-fire (LIF) neuronal model known as *spike response model* (SRM) (Gerstner and Kistler, 2002). Accordingly, each spiking neuron k outputs a binary signal $b_{k,t} \in \{0, 1\}$ at time $t = 1, \dots, T$, with $b_{k,t} = 1$ representing the firing of the spike and $b_{k,t} = 0$ an idle neuron at time t . Each neuron k receives inputs from a subset of neurons \mathcal{N}_k through directed links, known as *synapses*. Neurons in set \mathcal{N}_k are referred to as *pre-synaptic* with respect to neuron k ; while neuron k is said to be *post-synaptic* for any neuron $j \in \mathcal{N}_k$. For a fully-connected layered SNN, as assumed in the experiments of this paper, the set of pre-synaptic neurons, \mathcal{N}_k , for a neuron k in a given layer consists of the entire set of indices of the neurons in the previous layer.

Following the SRM, each neuron k maintains an internal analog state variable $o_{k,t}$, known as the *membrane potential*, over time t . The membrane potential $o_{k,t}$ evolves as the sum of the responses of the synapses to the incoming spikes produced by the pre-synaptic neurons, as well as of the response of the neuron itself to the spikes it produces. Mathematically, the evolution of the membrane potential is given as

$$o_{k,t} = \sum_{j \in \mathcal{N}_k} w_{k,j} \cdot (\alpha_t * b_{j,t}) + \beta_t * b_{k,t}, \quad (16)$$

where $w_{k,j}$ is a learnable synaptic weight between neuron $j \in \mathcal{N}_k$ and neuron k ; α_t represents a filter applied to the spiking signals produced by each pre-synaptic neurons; β_t is the filter applied to neuron’s k spiking output; and “ $*$ ” denotes the convolution operator.

Typical choices for synaptic filters include the first-order feedback filter $\beta_t = \exp(-t/\tau_{\text{ref}})$, and the second-order synaptic filter $\alpha_t = \exp(-t/\tau_{\text{mem}}) - \exp(-t/\tau_{\text{syn}})$, for $t = 1, 2, \dots$, with finite positive constants τ_{ref} , τ_{mem} , and τ_{syn} (Neftci et al., 2019). For the numerical results in the paper, we have adopted the first-order filter with $\tau_{\text{ref}} = 0.0195$. Each neuron k outputs a spike at time step t whenever its membrane potential crosses a fixed threshold ϑ , i.e.,

$$b_{k,t} = \Theta(o_{k,t} - \vartheta), \quad (17)$$

where $\Theta(\cdot)$ is the Heaviside step function. For our experiments, we set $\vartheta = 1$.

Supplementary A.2 Algorithmic Table for SpikeCP

The overall procedure of SpikeCP is summarized in Algorithm 1.

Algorithm 1: SpikeCP

Input : Pre-trained SNN classifier; calibration set \mathcal{D}^{cal} ; checkpoint candidates \mathcal{T}_s ; target accuracy level $p_{\text{targ}} \in (0, 1)$; target set size (informativeness) I_{th} ; and test input \mathbf{x}

Output : Adaptive set classification $\Gamma(\mathbf{x})$ at time $T_s(\mathbf{x})$ satisfying the reliability condition

Offline phase:

Compute the NC scores $s^t[i]$ for all calibration data points $i = 1, \dots, |\mathcal{D}^{\text{cal}}|$ in set \mathcal{D}^{cal} and for all checkpoints $t \in \mathcal{T}_s$

For each checkpoint $t \in \mathcal{T}_s$, obtain the threshold s_{th}^t as the $\lceil (1 - \alpha)(|\mathcal{D}^{\text{cal}}| + 1) \rceil$ -th smallest NC score in the set $\{s^t[i]\}_{i=1}^{|\mathcal{D}^{\text{cal}}|}$ with $\alpha = (1 - p_{\text{targ}})/|\mathcal{T}_s|$, if $\alpha \geq 1/(|\mathcal{D}^{\text{cal}}| + 1)$; otherwise set $s_{\text{th}}^t = \infty$

Test time:

for each checkpoint time $t \in \mathcal{T}_s$ **do**
 Generate the set predictor $\Gamma(\mathbf{x}^t)$ with threshold s_{th}^t
 if $|\Gamma(\mathbf{x}^t)| \leq I_{\text{th}}$ **then**
 Exit
 end

end

Set $\Gamma(\mathbf{x}) = \Gamma(\mathbf{x}^t)$ and stopping time $T_s(\mathbf{x}) = t$

Return: $\Gamma(\mathbf{x})$

Supplementary A.3 Additional Experiments on MINIST-DVS Dataset

In this section, we provide additional experimental results with the main aims of: (i) studying the impact of number of checkpoints and of the calibration set size on the performance of SpikeCP; and (ii) provide some numerical comparison with the adaptive point classifier – referred to as SP-SNN here – proposed in (Li et al., 2023b).

We start with a brief description of SP-SNN. SP-SNN defines a parameterized *policy* $\pi(\mathbf{x}|\phi)$, implemented using a separate artificial neural network (ANN), that maps the input sequence \mathbf{x} to a probability distribution $\pi(\mathbf{x}|\phi) = [\pi_1(\mathbf{x}|\phi), \dots, \pi_T(\mathbf{x}|\phi)]$ over the T time steps, where ϕ is the trainable parameter vector of the ANN. Accordingly, given input \mathbf{x} , the stopping time is drawn using the policy $\pi(\mathbf{x}|\phi)$ as $T_s(\mathbf{x}) \sim \pi(\mathbf{x}|\phi)$. The policy is optimized using reinforcement learning based on the training data, with the goal of maximizing an average reward that depends on the combination of latency and accuracy. Note that SP-SNN does not make use of calibration data. Furthermore, the SNN classifier can be potentially trained jointly with the

policy network, as described in (Li et al., 2023b), although in this paper we focus solely on pre-trained SNN classifiers.

In this work, we implement the policy network of SP-SNN as a recurrent neural network (RNN) with one hidden layer having 500 hidden neurons equipped with Tanh activation, followed by $T = 80$ output neurons with a softmax activation function. The RNN takes the time series data $\mathbf{x} = \{\mathbf{x}_t\}_{t=1}^T$ as input, and outputs a probability vector $\boldsymbol{\pi}(\mathbf{x}|\phi)$. The stopping time is chosen as $T_s(\mathbf{x}) = \arg \max \boldsymbol{\pi}(\mathbf{x}|\phi)$. The choice of a light-weight ANN architecture is dictated by the principle of ensuring that the size of the ANN is comparable to that of the SNN classifier. The same pre-trained SNN classifier is reused across all schemes.

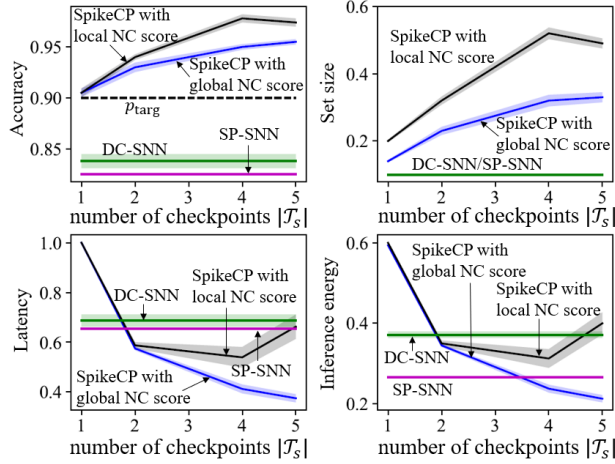


Figure 6: Accuracy, normalized latency, normalized set size (informativeness), and normalized inference energy as a function of number of checkpoints $|\mathcal{T}_s|$ for SpikeCP with local and global scores, as well as for DC-SNN and SP-SNN point classifiers, with $p_{\text{target}} = 0.9$, $|\mathcal{D}^{\text{cal}}| = 200$ and $I_{\text{th}} = 3$.

In Fig. 6, we show the performance of SpikeCP when using either local NC scores (11) or global NC scores (12) (see Sec. 4.1), as well as the performance of the DC-SNN and SP-SNN point predictors, as a function of the number of checkpoints $|\mathcal{T}_s|$, for $p_{\text{target}} = 0.9$, $|\mathcal{D}^{\text{cal}}| = 200$, and $I_{\text{th}} = 3$. The checkpoints are equally spaced among the T time steps, and hence the checkpoint set is $\mathcal{T}_s = \{T/|\mathcal{T}_s|, 2T/|\mathcal{T}_s|, \dots, T\}$. The metrics displayed in the four panels are the accuracy – probability $\Pr(c = \hat{c}(\mathbf{x}))$ for point predictors and probability $\Pr(c \in \Gamma(\mathbf{x}))$ for set predictors – along with normalized latency $\mathbb{E}[T_s(\mathbf{x})]/T$ and normalized, per-neuron and per-time step, inference energy $\mathbb{E}[S(\mathbf{x})]/(1000T)$. Note that the operation of SP-SNN and DC-SNN does not depend on the number of checkpoints, and hence the performance of these schemes is presented as a constant function.

By Theorem 1, SpikeCP always achieves negative reliability gap, while SP-SNN and DC-SNN fall short of the target reliability p_{target} in this example. Using global NC scores with SpikeCP yields better performance in terms of informativeness, i.e., set size, as well as latency and inference energy. The performance gap between the two choices of NC scores increases with the number of checkpoints, demonstrating that local NC scores are more sensitive to the Bonferroni

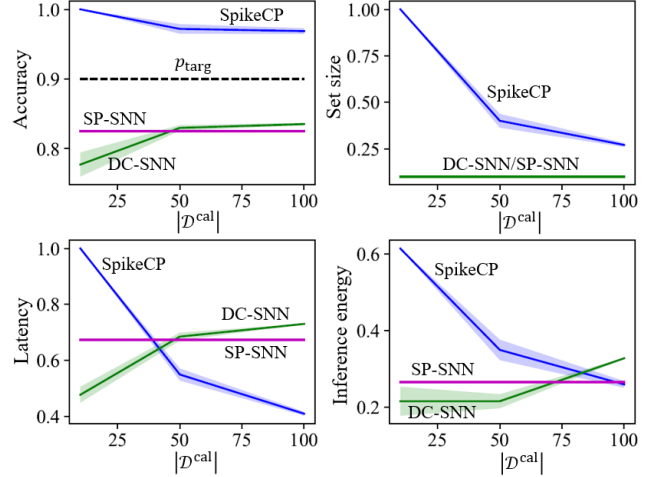


Figure 7: Accuracy, normalized latency, normalized set size (informativeness), and normalized inference energy as a function of number $|\mathcal{D}^{\text{cal}}|$ of calibration data points for SpikeCP with global NC scores, as well as for DC-SNN and SP-SNN point classifiers, with $p_{\text{target}} = 0.9$, $|\mathcal{T}_s| = 4$ and $I_{\text{th}} = 3$.

correction applied by SpikeCP (see Sec. 4). This is due to the lower discriminative power of local confidence levels, which yield less informative NC scores (see, e.g., (Fisch et al., 2020)). That said, moderate values of latency and inference energy can also be obtained with local NC scores, without requiring any coordination among the readout neurons. This can be considered to be one of the advantages of the calibration afforded by the use of SpikeCP.

With global NC scores, the number of checkpoints $|\mathcal{T}_s|$ is seen to control the trade-off between latency and informativeness for SpikeCP. In fact, a larger number of checkpoints improves the resolution of the stopping times, while at the same time yielding more conservative set-valued decision at each time step due to the mentioned Bonferroni correction.

In Fig. 7, we show the performance of SpikeCP with global NC scores, DC-SNN, and SP-SNN as a function of the number, $|\mathcal{D}^{\text{cal}}|$, of calibration data points, with $p_{\text{target}} = 0.9$, $|\mathcal{T}_s| = 4$, and $I_{\text{th}} = 3$. The general conclusions around the comparisons among the different schemes are aligned with those presented above for Fig. 6. The figure also reveals that SP-SNN outperforms DC-SNN in terms of accuracy when the calibration data set is small, while DC-SNN is preferable in the presence of a sufficiently large data set. This suggests that an extension of SP-SNN that leverages also calibration data may outperform both DC-SNN and SP-SNN (while requiring an additional ANN with respect to DC-SNN).

Finally, with a larger calibration data set, SpikeCP is able to increase the informativeness of the predicted set, while also decreasing latency and inference energy.

Supplementary A.4 Additional Experiments on CIFAR-10 Dataset

In this section, we provide additional experiments in order to verify the effectiveness of SpikeCP on the standard CIFAR-10 data set. To this end, we compare the performance of

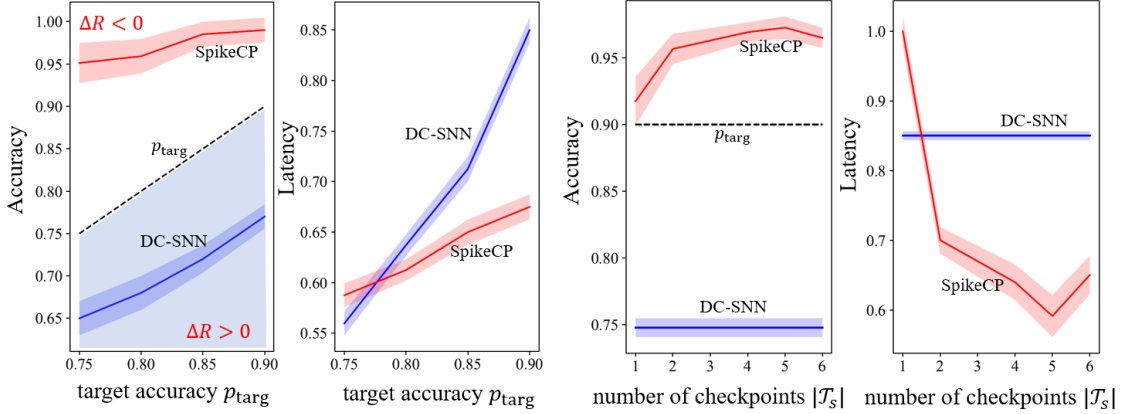


Figure 8: CIFAR-10 experiments: Accuracy ($\Pr(c = \hat{c}(\mathbf{x}))$ for DC-SNN and $\Pr(c \in \Gamma(\mathbf{x}))$ for SpikeCP), and normalized latency $\mathbb{E}[T_s(\mathbf{x})]/T$ for the proposed SpikeCP set predictor and DC-SNN as a function of target accuracy p_{targ} with $|\mathcal{D}^{\text{cal}}| = 50$, $p_{\text{targ}} = 0.9$, $|\mathcal{T}_s| = 4$ and $I_{\text{th}} = 3$, on CIFAR-10 Dataset.

SpikeCP with the point predictor, DC-SNN, in terms of reliability and inference latency.

The CIFAR-10 dataset consists of 60,000 32×32 color images that are divided into 10 classes, with 6000 images per class. There are 50,000 training images and 10,000 test images. We use $|\mathcal{D}^{\text{cal}}| = 50$ calibration samples, which are obtained by randomly selecting 50 data points from the test set. We adopt a ResNet-18 architecture in which conventional neurons are replaced with SRM neurons (Fang et al., 2021). Each example is repeatedly presented to the SNN for $T = 80$ times. We use global score for SpikeCP, and set the threshold as $I_{\text{th}} = 3$.

In Fig. 8, we demonstrate the accuracy and normalized latency of SpikeCP and DC-SNN as a function of the target accuracy p_{targ} and of the number of checkpoints $|\mathcal{T}_s|$. The general conclusions reached from the analysis of these results are aligned with the insights obtained from the experiments reported in the main text. In particular, SpikeCP is seen to guarantee reliability regardless of the target accuracy and of the number of checkpoints, while DC-SNN cannot meet the target accuracy. Furthermore, the inference latency decreases with a larger number of checkpoints due to the larger granularity of the stopping times allowed for SpikeCP, and meanwhile producing more conservative set due to the Bonferroni correction imposed for each checkpoint time.